Nonadiabatic Dynamics of Excited Hg(^{3}P$_1$) in Ar Matrixes[†]

Germán Rojas-Lorenzo and Jesús Rubayo-Soneira

Departamento de Física General y Matemáticas, Instituto Superior de Ciencias y Tecnología Nucleares, La Habana, Cuba

Sebastián Fernández Alberti*

Centro de Estudios e Investigaciones, Universidad Nacional de Quilmes, Roque Sáenz Peña 180, Bernal (B1876BXD), Argentina

Majed Chergui

Institut de Physique de la Matière Condensée, Faculté des Sciences, BSP, Université de Lausanne, CH-1015 Lausanne, Switzerland

The absorption and emission spectra of the ^{3}P$_1$−^{1}S$_0$ transition of a Hg atom embedded in solid argon have been simulated using the molecular dynamics with quantum transitions algorithm to consider the nonadiabatic transitions between the three adiabatic states. The simulations also take into account the zero-point fluctuations at the experimental temperature of 4 K using a temperature correction that mimics them. The simulated spectra show fair agreement with the experimental data for the absolute energies and very good agreement for the absorption-emission Stokes shift. The absorption band consists of the contribution due to absorption of the three degenerate atomic states. The simulations of the emission spectrum, with inclusion of nonadiabatic couplings, lead to a single emission band stemming from the lowest adiabatic surface. When running the simulations without consideration of the nonadiabatic coupling, the simulated absorption and emission spectra exhibit three bands separated by hundreds of cm^{-1}, in total disagreement with the experiment. This shows that photoexcitation of Hg(^{3}P$_1$) in Ar matrixes is characterized by the medium-induced nonadiabatic couplings among its adiabatic states.

I. Introduction

The study of open-shell atoms in rare gas solids allows the exploration of the effect of solvents on the dynamics of the electron orbital. This issue is of importance in the case of the P states of atoms, as electronic degeneracies or near degeneracies arise, with the possibility of a breakdown of the Born−Oppenheimer approximation. The nature of P states of atoms in rare gas solids has been addressed mostly by electronic spectroscopy (absorption and luminescence) in the case of pure electronically excited rare gas solids[1] and, mainly of metal atoms, such as Mg,[2] Zn,[3] Hg,[4−7] Cd,[8] alkali atoms,[9,10] Au,[11] and Ag.[12]

Over the past few years, Hg−rare gas as van der Waals complexes or as matrixes has emerged as a model system for the study of state splittings and nonadiabatic couplings due to the local environment around the Hg atom, thanks to detailed electronic spectroscopic studies in both absorption and emission studies. In the Hg−Rg complexes, the excitation region of the Hg(^{3}P$_1$−^{1}S$_0$) transition shows two distinct bands, one red-shifted (labeled A) and the other blue-shifted (labeled B), with respect to the atomic line. The former has been assigned to the electronic state associated with the projection $\Omega = 0$ of the Hg electronic angular momentum $J = 1$ onto the interatomic axis, whereas the blue-shifted component has been assigned to the degenerate

$\Omega = \pm 1$ states.[13−16] From the analysis of these spectra, interatomic potentials were determined for the ground and the A and B excited states of the Hg−Rg (Rg = Ne, Ar, Kr, and Xe) potentials. These empirically determined interactions were used to model the potential surfaces of Hg−Rg$_n$ clusters.[17,18] In this case, the ground-state potential surface correlating asymptotically to Hg(^{1}S$_0$) is simply written as the sum of pairwise interactions. For the excited-state Hg(^{3}P$_1$) involving an electronic angular momentum different from zero, the quantization axis cannot be defined simultaneously along each Hg−Rg bond (except in the case of a collinear configuration). If one chooses a particular quantization axis Z in the molecular frame to which the electronic wave functions $|J, \Omega\rangle$ are referred, the A- and B-state wave functions for a particular Hg−Rg pair will be mixed by the axis-switching rotation, which brings the Hg−Rg bond onto the quantization axis. The result of this mixing is that the excited-state potential energy surface is no longer the sum of individual A (or B) interactions. In addition, off-diagonal matrix element of the electronic Hamiltonian is generated. This diabatic potential energy matrix can then be diagonalized for each nuclear configuration to obtain the adiabatic potential energy surfaces and the corresponding nonadiabatic couplings. It is therefore possible to calculate the complete manifold of electronically excited potential energy surfaces and the interelectronic couplings for clusters of any size. In doing so, one neglects the three-body and higher-order interactions and assumes that the properties of the electronic angular momentum

---

[†] Part of the special issue "A. C. Albrecht Memorial Issue".
* Corresponding author.

J_e are conserved within the complex. Zúñiga et al.[18] applied this procedure to the analysis of the fluorescence-excitation spectrum of a Hg$-$Ar$_2$ complex[16,19,20] and obtained good agreement with the experimental data.

The spectroscopy of Hg-doped$-$rare gas solids in the region of the Hg(^{3}P$_1$$-^1S_0$) transition has been investigated in detail by Crépin and Tramer[4] and Helbing et al.[7] Featureless bands progressively blue-shifted with respect to the gas phase were observed in Ar and Kr matrixes, while the absorption band in solid Xe exhibited a triplet structure. The emission spectra showed a weak Stokes shift and a near mirror image between absorption and emission bands in Ar and Kr, whereas the Stokes shift and the emission band were much larger in solid Xe.

Assuming additivity of pair potentials and a rigid lattice model with 18 rare gas atoms, Crépin and Tramer[4,6] qualitatively interpreted the absorption and emission spectra of Hg-doped$-$rare gas matrixes, suggesting that excited Hg atoms are little displaced from their ground-state equilibrium position in Ar or Kr matrixes, while they tend to form a 1:1 complex with a Xe atom in solid Xe. In so doing, they considered only two possible deformations of the matrix: either a totally symmetric breathing of the cage or a displacement of the Hg atom from its central position. McCaffrey and co-workers applied a similar approach with more accuracy to the case of the absorption and emission spectra of Cd and Zn atoms in rare gas matrixes.[8,21] To interpret the emission, they introduced characteristic deformations of the matrix atoms such as 4-atom or 6-atom "body" and "waist" modes in a static fashion, i.e., by minimizing the total energy along a specific deformation coordinate.

Although these approaches are useful in delivering insight on the spectroscopy, they cannot provide the details of the relaxation dynamics of the system under study. One of the reasons is that they do not consider the nonadiabatic couplings among the degenerate Hg states. The procedure used by Beswick and co-workers[18] for Hg$-$Rg$_n$ complexes, combined with molecular dynamics simulations, contains all the ingredients that are needed to treat the case of electronically excited Hg atoms in rare gas matrixes (see below). Indeed, not only does it provide the diagonal matrix elements (i.e., the energies), but it also provides the nondiagonal ones that are essential for the interstate couplings, which govern the energy relaxation pathways of the system and are caused by nonadiabatic couplings. In particular, a real-time picture of the energy relaxation process and the accompanying structural changes in the matrix would provide much insight into the way energy is funneled within the system and from the impurity to the lattice.

The issue of nonadiabatic effects in the dynamics of atomic impurity-doped rare gas solids as models for condensed-phase nonadiabatic dynamics has been the center of much interest over the past few years. Gerber and co-workers[22] have treated semiclassically the dynamics of nonadiabatic transitions between degenerate electronic states originating from the ground-state (P-type) F atoms in rare gas solids. They found that the p orbital reorientation dynamics occurs at very short time scales (tens of fs) and is dominated by nonadiabatic mechanisms. In addition, lattice vibrations of particular symmetry are effective in inducing the p orbital reorientation. Ideally, such calculations can be effectively tested by comparison with the absorption and emission spectra of the species of interest. This was not possible in the case of F atoms because the simulations by Gerber and co-workers concerned only the ground state; their main interest was to address the issue of chemical reactions in the condensed phase. Previously, Last et al.[23] had generated the excited states of the Cl impurity in solid Xe using the DIM (diatomics-in-

molecule) method and calculated its absorption spectrum. Schwentner and co-workers[12] investigated the steady-state spectroscopy and ultrafast relaxation dynamics of silver atoms in Xe matrixes. In this case, the s$-$p excitation of the Ag atom leads to a dynamics Jahn$-$Teller effect, which in addition to the spin$-$orbit coupling, removes the degeneracy of the p state. Potential surfaces for the 5s and 5p states in the vibrationally distorted O_h symmetry of the Xe matrix were constructed by a numerical diagonalization of the Hamiltonian, using parameters derived from the absorption and emission spectra. Only two deformation modes were considered for the calculation of the Stokes shift, and good agreement with the experiment was found.[12] Although such calculations[8,12,21] do provide a lot of insight into the relaxation process, they impose restrictions to the system in terms of deformation type and do not deliver time scales for the process.

The purpose of the present paper is to simulate the absorption and emission spectra of Hg atoms in Ar matrixes, using the procedure used in refs 17 and 18 and the molecular dynamics with quantum transitions (MDQT) method developed by Tully[24,25] to treat the nonadiabatic transitions between the states. In that sense, no restrictions are imposed on the system, and the deformations and time scales inherent to the relaxation process are found by the energy minimization of the system.

II. Methodology

II.A. The MDQT Method. Briefly, the MDQT method treats the electronic degrees of freedom quantum mechanically, whereas the motions of the nuclei are treated classically. The nuclei evolve on a potential energy surface (PES) that is defined by a single electronic state at a given time. Hops from one electronic state to another are governed by the coefficients of the electronic wave function.

In the present work, the electronic wave function is written as:

$$\psi(r,R,t) = \sum_i c_i(t)\phi_i(r;R) \tag{1}$$

where r and R are the electronic and nuclear coordinates, respectively, and $\phi_i(r;R)$ is the eigenstate of the electronic Hamiltonian $H^{\text{Hg}-\text{Ar}}$ with energy $E_i(R)$,

$$H^{\text{Hg}-\text{Ar}}(r;R)\phi_i(r;R) = E_i(R)\phi_i(r;R) \tag{2}$$
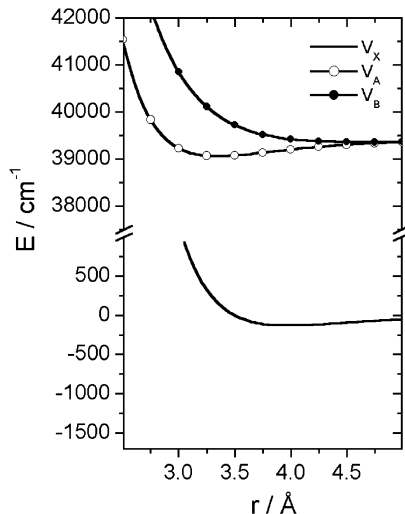
The coefficients $c_i(t)$ evolve in time according to

$$i\hbar\dot{c}_i(t) = c_i(t)E_i - i\hbar\sum_j c_j(t)\dot{R}d_{ij} \tag{3}$$

where

$$d_{ij} = \langle\phi_i(r;R)|\nabla_R\phi_j(r;R)\rangle \tag{4}$$

is the nonadiabatic coupling vector.

II.B. Potential Energy Surfaces and Couplings. The ^{3}P state of mercury splits into two states in the Ar$-$Hg complex, $^3\Pi$ and $^3\Sigma$, differing by the projection of the excited orbital onto the interatomic axis and by their bonding energies. The further mixing due to the spin$-$orbit coupling gives rise to the $A(0^+)$ = $|^3\Pi\rangle$ and the $B(1) = (|^3\Pi\rangle + |^3\Sigma\rangle)/2$ stationary states. The A state is allocated to the $|J = 1, \Omega = 0\rangle$ electronic state associated with the projection $\Omega = 0$ of the mercury electronic angular momentum $J = 1$ onto the interatomic axis. Correspondingly, the B state is allocated to the $|J = 1, \Omega = \pm1\rangle$ state of the complex. Their potential curves, $V_A(R)$ and $V_B(R)$,

Nonadiabatic Dynamics of Hg(^{3}P$_1$) in Ar Matrixes

J. Phys. Chem. A, Vol. 107, No. 40, 2003 **8227**

Figure 1. Potential energy curves of Hg−Ar for the ground state and the A and B excited states, denoted by V_x, V_A, and V_B, respectively.[18]

TABLE 1: Hg−Ar and Ar−Ar Potential Parameters

	D_o (cm^{-1})	β (Å^{-1})	r_e (Å)
Ar−Hg(^{3}P$_1$) V_B[18]	51.57	1.116	4.66
Ar−Hg(^{3}P$_1$) V_A[18]	353.63	1.541	3.34
Ar−Hg(^{1}S$_0$) V_x[18]	130.25	1.448	3.98

	ϵ (cm^{-1})	σ (Å)
Ar−Ar[26]	366.96	3.39

have been deduced experimentally[13−17] and are represented by the Morse pair potentials along with ground-state potential V_x. The potential parameters[13−18,26] we used are given in Table 1, and the resulting potential curves are shown in Figure 1. Using the J,Ω basis seems more realistic because of the important spin−orbit coupling in Hg−Ar.

The total interaction Hamiltonian, $H^{\text{Hg}-\text{Ar}}$, for the ground electronic state correlating asymptotically to Hg(^{1}S$_0$) is written simply as the sum of pairwise interactions. However, as already mentioned, this cannot be applied to the excited states involving an electronic angular momentum different from zero (e.g., Hg(^{3}P$_1$)) where the quantization axis cannot be defined simultaneously along each Hg−Ar bond. To this end, we follow the model proposed by Beswick et al.:[18,27] $|J,\Omega\rangle_Z$ denotes the electronic wave functions of the mercury atom with projection Ω on axis Z and $|J,\Omega\rangle_{Zk}$ is the corresponding wave function with projection Ω on the Hg···Ar$_k$ axis. Equation 5 shows the transformation

$$|J,\Omega\rangle_Z = \sum_{\Omega'} D^{J*}_{\Omega\Omega'}(\phi_k,\theta_k,0)|J,\Omega'\rangle_{Z_k} \quad (5)$$

where $D^{J*}_{\Omega\Omega'}(\phi_k,\theta_k,0)$ is the Wigner rotation matrix and θ_k and ϕ_k are the polar angles that define the orientation of the particular Hg···Ar, with respect to axis Z. The matrix elements of the Hg···Ar$_k$ diatomic Hamiltonian $H^{\text{Hg}-\text{Ar}_k}$ in the $|J,\Omega\rangle_Z$ representation is written as

$$\langle J,\Omega'|H^{\text{Hg}-\text{Ar}_k}|J,\Omega''\rangle_Z = \sum_{\Omega} D^{J}_{\Omega'\Omega}(\phi_k,\theta_k,0)D^{J*}_{\Omega'\Omega}(\phi_k,\theta_k,0)V_\Omega(R_k) \quad (6)$$

where

$$V_\Omega(R_k) = \langle J,\Omega|H^{\text{Hg}-\text{Ar}_k}|J,\Omega\rangle_{Z_k} \quad (7)$$

are the potentials denoted as V_A and V_B (Figure 1).

This procedure is repeated for each Hg···Ar bond in the whole system, leading to nondiagonal elements in the total electronic Hamiltonian of the system. The total electrostatic interaction Hamiltonian of Hg atom with n_{Ar} argon atoms in the solid is written as:

$$H^{\text{Hg}-\text{Ar}} = \sum_{k=1}^{n_{\text{Ar}}} H^{\text{Hg}-\text{Ar}_k} \quad (8)$$

We then diagonalize the resulting *diabatic* matrix of $H^{\text{Hg}-\text{Ar}}$ to obtain the *adiabatic* energies E_i of eq 2. The practical implementation of this procedure is given in the Appendix and is equivalent to the one proposed by Batista and Coker.[28,29]

Our treatment is limited to energies and does not consider the transition dipoles for the different Ω states. The aim of this work is to stress the role of nonadiabatic couplings in the description of the energetics of the system at the beginning (absorption), during, and end (emission) of the structural relaxation process. Although a full treatment should also include a simulation of the intensities, it does not affect the emission, which stems from only one state (see below), and its effect on the absorption spectrum is not significant, as we will see below.
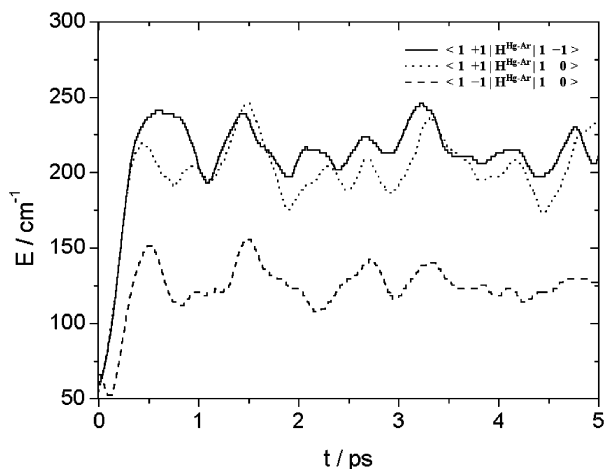
II.C. Molecular Dynamics Simulations. The calculations described in this work were carried out with minimum image convention for a system composed of 1 Hg atom and 499 Ar atoms. The number of Ar atoms corresponds to a box large enough to avoid size effects, at least at the short time scales of the dynamical simulations. The Hg atom was initially placed at a monosubstitutional site of the argon matrix.

As the first step in our calculations, the system was equilibrated in the electronic ground state for 400 ps at an effective temperature T'. The last 200 ps were used to collect a set of initial positions and momenta for the subsequent simulations in the excited states. The stored configurations fulfill the classical Franck principle for the electronic transition at $\lambda_{\text{exc}} = 246$ nm from the ground state to one of the three possible adiabatic excited states defined by eq 2 and asymptotically correlated to Hg(^{3}P$_1$). At this energy, each excitation event is found to reach one of these states. In fact, the population produced in the three states by all the excitation events remains constant.

One hundred trajectories of 10 ps each were run from these initial configurations by Franck−Condon switching to each of the three excited states. The propagation time was sufficient to achieve a convergence of the final electronic state populations in time. To represent the vibrational amplitudes of the Ar atoms, we adjusted their velocities to an effective temperature T'. The effective temperature is chosen in such a way that the classical probability distribution for a harmonic oscillator matches the quantum probability distribution in the limit $\hbar \rightarrow 0$ and is given by the equation:

$$T' = \frac{\hbar\omega}{2k_B}\left(\tanh\left(\frac{\hbar\omega}{2k_BT}\right)\right)^{-1} \quad (9)$$

where the experimental temperature is $T = 4$ K[4,7] and $\hbar\omega = 67$ cm^{-1}, yielding $T' = 49$ K. Indeed, at constant temperature and for harmonic oscillators (our case), we simulated a canonical ensemble whose classical distribution matches the quantum distribution. This way of introducing quantum corrections (the so-called thermal harmonic quantum correction) in the classical treatment was first proposed by Bergsma et al.,[30] and it is commonly and successfully used in molecular dynamics simulations of photoinduced processes of small molecules in the rare

Figure 2. Average overall trajectories of the diabatic couplings vectors, $\langle J = 1, \Omega | H^{\text{Hg}-\text{Ar}} | J = 1, \Omega' \rangle$, as a function of time.

gas matrixes.[31−33] Nevertheless, to estimate the role of this correction in the simulated spectra, we will also present our simulations at an effective temperature of $T' = 4$ K.

The equilibration of the system at the desired temperature T' is performed using the velocity method[34] in which velocities are scaled at each time step by a factor λ defined as
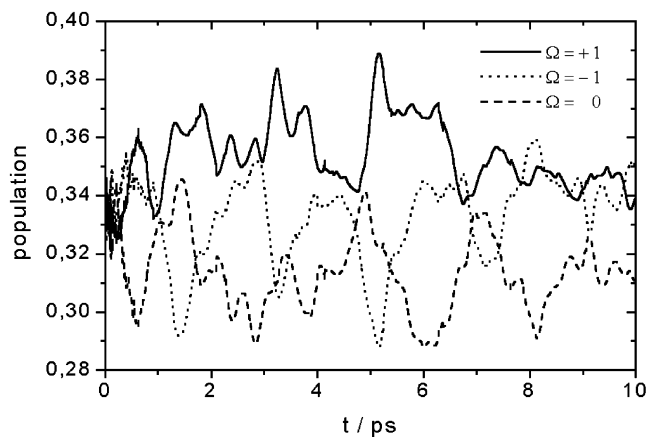
$$\lambda = \left[1 + \frac{\Delta t}{2\tau}\left(\frac{T'}{T} - 1\right)\right]^{1/2} \qquad (10)$$

where Δt is the time step, T the current temperature of the system, and T' the target temperature. A relaxation constant, τ of 0.4 ps, was used. This value was chosen to ensure that the simulations were run at constant temperature.
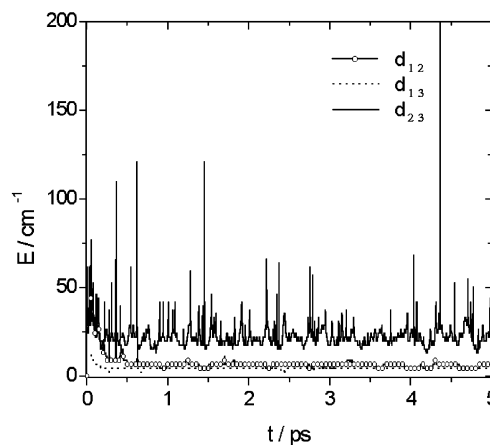
III. Results and Discussion

We have performed simulations of the excitation process of Hg atom in a cryogenic argon matrix at 246 nm, which is associated with the Hg($^3P_1$−$^1S_0$) transition. The MDQT method was used in the adiabatic representation of the excited electronic states, i.e., the nuclei move on potential energy surfaces obtained from eq 2. However, the MDQT method is valid for both adiabatic or diabatic representations.[35] We could choose diabatic potential energy surfaces given by the diagonal terms of the $H^{\text{Ar}-\text{Hg}}$ diabatic matrix (see section II.B., paragraph 2). The advantage of using one representation or the other depends on the relative strength and persistence through time of the diabatic $H^{\text{Ar}-\text{Hg}}$ nondiagonal terms and adiabatic couplings (eq 4). Both representations have been used in this work.

Figure 2 shows the average overall trajectories of the *diabatic* couplings among the $|J = 1, \Omega = 0\rangle$, $|J = 1, \Omega = +1\rangle$, and $|J = 1, \Omega = -1\rangle$ states as a function of time. The description in terms of *diabatic states*, which are defined in the diatomic frame, is however still valid in the matrix. Indeed, what is shown in Figures 2 and 3 is the projection of the adiabatic states of the matrix on the diabatic states of the diatom. In Figure 2, it can be seen that the couplings among diabatic potential energy surfaces persist at all times so that nonadiabatic transitions are possible throughout the duration of the dynamics. As a matter of fact, the population of the individual diabatic excited states fluctuates close to ∼33%, as can be seen from Figure 3. Tully et al.[36] pointed out that this situation leads to an unsatisfactory performance of the MDQT algorithm. Whenever the couplings among potential energy surfaces do not vanish for arbitrarily long times, MDQT introduces nonphysical loss of coherence. In principle, if the electronic population is plotted as a function

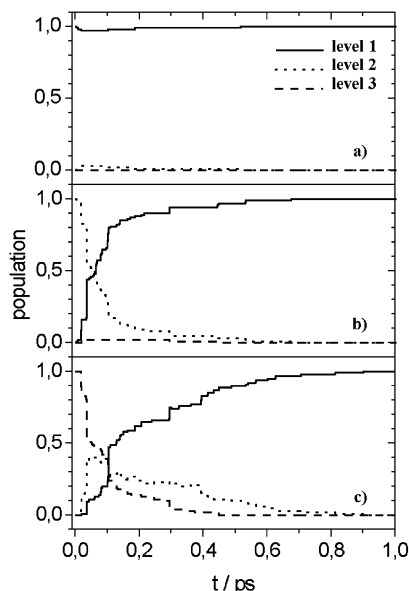**Figure 3.** Population of the excited diabatic states as a function of time.

Figure 4. Average overall trajectories of the adiabatic couplings vectors d_{ij}, as a function of time. The states 1, 2, and 3 are associated with the different adiabatic states in ascending order of energy.
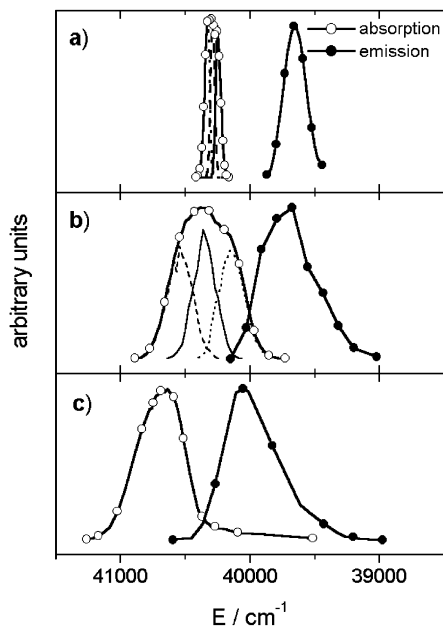
of time, one should observe oscillations of the population due to its exchange caused by the nonadiabatic couplings. However, MDQT fails in this case, as it shows damped oscillations, which are attributed to the fact that the different trajectories exhibit a different history of random hops, causing the ensemble to lose coherence over time, in the sense that the phase of the electronic coefficients is lost.

On the other hand, the nonadiabatic couplings decrease very fast during these dynamics. This can be seen in Figure 4, where we plotted the average overall trajectories of the *nonadiabatic* couplings vectors (eq 4) as a function of time. The levels 1, 2, and 3 are associated with the different adiabatic states in ascending order of energy. Except for the d_{23} coupling vector, the others are relatively insignificant beyond the first ps of the dynamics. The spiking behavior is due to the fact that levels 2 and 3 are almost degenerate, or at least that the coupling parameter is larger than their energy separation (see also Figure 7). Furthermore, the d_{23} coupling vector does not play a significant role in the dynamics at longer times because the entire population is located in adiabatic level 1 after ∼1 ps of the dynamics. This is shown in Figure 5, which displays the populations of adiabatic excited states as a function of time. The averages overall trajectories starting at the adiabatic states 1, 2, and 3 are shown in frames a, b, and c, respectively. All the trajectories end up in state 1, which is the lowest-energy state, in less than 1 ps. Starting on state 2 leads to a relaxation of the population to state 1 on the time scale of 100 fs. Starting on state 3 leads to a rapid relaxation to state 2 on a similar time

Nonadiabatic Dynamics of Hg($^3P_1$) in Ar Matrixes

J. Phys. Chem. A, Vol. 107, No. 40, 2003 **8229**

Figure 5. Populations of adiabatic excited states as a function of time. The averages over trajectories starting at the different adiabatic states 1, 2, and 3 are shown separately in a, b, and c, respectively.

Figure 6. Simulated absorption and emission spectra at effective temperatures of 4 K (a) and 49 K (b), compared to the experimental absorption and emission bands (c) in the energy region associated to the Hg($^3P_1-^1S_0$) transition. The decomposition of the absorption band in its three quasi-degenerate components (see text) is also shown.

TABLE 2: Comparison of the Experimental and Calculated Absorption and Emission Energies (E) and of the Corresponding Line Widths (Γ)[a,b]
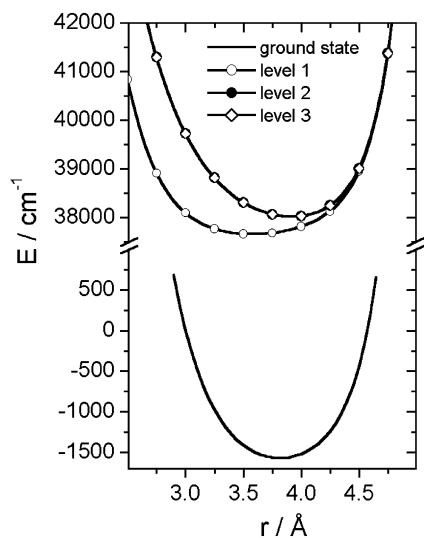
	experiment[4]	simulation $T' = 49$ K	simulation $T' = 4$ K
E_{abs}	40 650	40 372	40 299
Γ_{abs}	430	560	131
E_{ems}	39 940	39 675	39 663
Γ_{ems}	400	480	209
ΔE_{Stokes}	710	697	636

[a] ΔE_{Stokes} is the absorption-emission Stokes shift. [b] All entries in cm^{-1}.
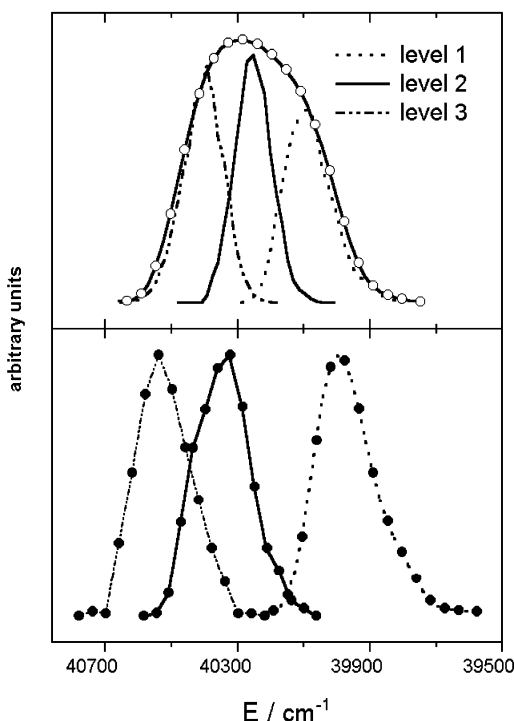
structure of solid Ar is not perturbed by the presence of the impurity. Because the absorption spectrum consists of transitions from the ground state to the three degenerate diabatic states ($J = 1$, $\Omega = 0, \pm 1$), we show the decomposition of the absorption band in three subbands corresponding to the latter. In the case of the emission spectrum, the final configurations resulting from simulations in the excited states were considered. These simulations obviously include the nonadiabatic coupling and result in the lowest state 1 being populated (Figure 5). The experimental spectra of Hg in solid Ar obtained by Crépin and Tramer[4] are shown in Figure 6c. We also show in Figure 6a the spectra simulated at an effective temperature of 4 K. The energies at band maxima, absorption-emission Stokes shifts, and bandwidths from the experiment and the present work are compared in Table 2. Although a fair agreement is achieved for the absolute energies with the simulations showing a red-shift of 200−300 cm^{-1} with respect to the experiment, good agreement is obtained for the absorption-emission Stokes shift. However, overall, the simulations at $T' = 49$ K give a better agreement with the experiment. This is more so when we come to the bandwidths, which are too narrow at $T' = 4$ K. However, the bandwidths are larger by 20−30% than the experiment in the simulations at $T' = 49$ K. As mentioned above, the emission band consists of the contribution of the lowest excited adiabatic level 1 alone, because all trajectories terminate in this state. However, the expansion of this adiabatic state onto the diabatic basis reveals it to be a mixture of the three different diabatic states (consistent with Figure 3). Although the electronic population of diabatic states remains significant for long times in all the states, the electronic population of the adiabatic states quickly flows into a single state. The trajectories get trapped in the minimum of the level 1 within the first ps of dynamics (Figure 5).

Figure 7 shows the adiabatic PES obtained from eq 2 using $\langle J\Omega|H^{Hg-Ar}|J'\Omega'\rangle$ matrix elements given by eq 6. They are obviously very different from the PES of the isolated Hg−Ar complex (Figure 1) and are also strongly coupled, underlining the influence of the environment on the electronic states of the Hg−Ar system.

To stress the importance of the couplings between the different excited states correlating asymptotically to Hg($^3P_1$), we have also performed the simulations in the adiabatic approximation, i.e., without considering any coupling among states. This means we start off with the gas-phase potential curves of Figure 1 and add the contribution of the Ar environment by pairwise summation of Hg−Ar and Ar−Ar interactions. Figure 8a shows the resulting simulated absorption spectrum which, as expected, is the same as in Figure 6b, because the ground state is projected onto the three excited degenerate states regardless of whether they are coupled. However, the emission spectrum (Figure 8b) is very different and exhibits three bands, in complete disagreement with the

scale, which then feeds the population to state 1. There seems to be little or no relaxation from state 3 to state 1, in agreement with the vanishingly small adiabatic coupling vectors (Figure 4). Thus, this situation can suitably be treated with the MDQT method in the adiabatic representation.

Figure 6b shows the resulting absorption and emission spectra resulting from our simulations. Both spectra were calculated as the histograms of energy differences between the initial (ground state for absorption, excited adiabatic states for emission) and the final state or states (excited adiabatic states for absorption, ground state for emission), which implicitly takes into account the instantaneous gradient of the excited-state potential. The equilibration of population in the ground state shows that the matrix has a cage radius of ~3.8 Å, which means that the lattice

Figure 7. Adiabatic potential energy surfaces for the Hg−Ar interaction of Hg in an argon matrix as a function of the Hg−Ar distance.

Figure 8. (a) Absorption and (b) emission bands in the energy region associated with the Hg($^3P_1$−$^1S_0$) transition resulting from molecular dynamics simulations using the adiabatic approximation, i.e., without consideration of the couplings between the electronic states.

experimental data (Figure 6c) because the population funnels down the three states, excluding the possibility of nonradiative transitions among them, which are mediated by the nonadiabatic couplings. This demonstrates strikingly that the photoexcitation process of Hg($^3P_1$) in a cryogenic argon matrix is a nonadiabatic process where medium-induced couplings among different electronic states must be considered.

The lowest excited adiabatic level 1 has a minimum at shorter Hg−Ar distances than the other levels, in particular of the ground state, so that at the end of the dynamics the cage should experience a contraction, according to Figure 7. We have analyzed in detail the trajectories of the matrix atoms and of the Hg impurity. The results are not shown here, but we could not observe a significant deformation of the cage because of the large error bars which characterize the simulated trajectories.

A weak deformation is, however, in line with the weak Stokes shift and the near-mirror image between absorption and emission line shapes, which are experimentally observed, pointing to little lattice reorganization around the impurity.

IV. Conclusions

The absorption and emission line shapes of the Hg atom in rare gas matrixes have been, for the first time, simulated using molecular dynamics with quantum transitions to take into account the nonadiabatic transitions among the states correlating to the $^3P_1$ state of Hg. The excited-state potential surfaces were generated from the empirically determined Hg*−Ar pair interactions by a procedure applied by Beswick and co-workers to the case of Hg−Ar$_n$ complexes.[18] The absorption band appears to be a triplet transition to the degenerate levels of the $^3P_1$ atomic state. The simulations using the adiabatic potential surfaces show that emission stems from only one adiabatic potential surface, which is populated by nonadiabatic transitions from the other two in less than 1 ps. The calculated absorption-emission Stokes shift is in very good agreement with the experimentally determined Stokes shift, but the absolute absorption and emission energies are systematically red-shifted by about 300 cm^{-1}. The origin of this discrepancy may be due to the assumption of pairwise additivity in the matrix. As the interaction between Hg and the rare gas atom increases, this discrepancy should also increase, and a test of this conjecture would be to apply the case of Kr matrixes. Indeed, in this case, the spectra and the analysis made by Crépin and Tramer[4,6] suggest a situation quite similar to solid Ar, except for the stronger Hg−Kr interaction. Extending the simulations to the case of Hg in solid Xe is a fascinating prospect as the experimental data suggests a dramatic rearrangement of the local structure with the Hg atom forming a complex with a Xe atom. Similar results have been obtained for Ag in Xe matrixes, and it would be interesting to test the generality of the process of lattice relaxation.[12] Work is now in progress to treat the case of Hg atoms in Kr and Xe matrixes.

Appendix

The transformation (eq 5) that leads to the $H^{Hg−Ar_k}$ expressed as indicated in eq 6 is implemented as a combination of axis-switching double rotations:

A rotation from the electronic states defined in a reference frame (X_k, Y_k, Z_k) with its Z_k axis parallel to the Hg···Ar$_k$ bond vector to the fixed reference frame (X', Y', Z') of the laboratory according to the transformation

$$D[H^{Hg−Ar_k}]D^{-1} \qquad (A1)$$

with D the Cartesian rotation matrix

$$D = \begin{bmatrix} \sin(\alpha) & 0 & \cos(\alpha) \\ -\cos(\beta)\cos(\alpha) & \sin(\beta) & \cos(\beta)\sin(\alpha) \\ -\sin(\beta)\cos(\alpha) & -\cos(\beta) & \sin(\beta)\cos(\alpha) \end{bmatrix} \qquad (A2)$$

where α is the angle of the Hg···Ar$_k$ vector with respect to the X' axis and β is the angle between its projection in the $Y'Z'$ plane and the Y' axis.

Nonadiabatic Dynamics of Hg(^{3}P$_1$) in Ar Matrixes

J. Phys. Chem. A, Vol. 107, No. 40, 2003 **8231**

A rotation of $H^{\text{Hg}-\text{Ar}_k}$ expressed in the fixed reference frame (X',Y',Z') to an arbitrary body fixed reference frame (X,Y,Z) (we chose a reference frame with its Z axis parallel to an arbitrary Hg$\cdots$Ar$_k$ bond vector) according to:

$$D^{-1}[H^{\text{Hg}-\text{Ar}_k}]D \tag{A3}$$

with D defined as (A2) and where α and β angles are the angle of the Hg$\cdots$Ar$_k$ chosen to define the reference frame with respect to the X' axis and the angle of its projection in the Y',Z' plane with the Y' axis, respectively.

References and Notes

(1) Boursey, E.; Castex, M.-C.; Chandrasekharan, V. *Phys. Rev. B: Condens. Matter* **1977**, *B16*, 2858.

(2) McCaffrey, J. G.; Ozin, G. A. *J. Phys. Chem.* **1994**, *101*, 10354.

(3) Bracken, V. A.; Gürtler, P.; McCaffrey, J. G. *J. Chem. Phys.* **1997**, *107*, 5290.

(4) Crépin, C.; Tramer, A. *J. Chem. Phys.* **1992**, *97*, 4772.

(5) (a) Chergui, M.; Crépin, C.; Hebert, T.; Tramer, A. *Chem. Phys. Lett.* **1992**, *197*, 467. (b) Crépin, C.; Chergui, M.; Hebert, T.; König, L.; Martin, P.; Tramer, A. *J. Phys. Chem.* **1994**, *98*, 3280.

(6) Crépin, C.; Legay, F.; Legay-Sommaire, N.; Tramer, A. *Trends Chem. Phys.* **1999**, *7*, 111.

(7) (a) Helbing, J.; Haydar, A.; Chergui, M. *Chem. Phys. Lett.* **1999**, *310*, 43. (b) Helbing, J.; Chergui, M.; Haydar, A. *J. Chem. Phys.* **2000**, *113*, 3621.

(8) Healy, B.; McCaffrey, J. G. *J. Phys. Chem.* **2000**, *A104*, 3553 and references therein.

(9) Balling, L. C.; Wright, J. J. *J. Chem. Phys.* **1983**, *79*, 2941 and references therein.

(10) Tam, S.; Fajardo, M. E. *J. Chem. Phys.* **1993**, *99*, 854.

(11) Roser, D.; Pellow, R.; Eyring, M.; Vala, M.; Lignieres, J.; Rivoal, J. C. *Chem. Phys.* **1992**, *166*, 393 and references therein.

(12) (a) Bammel, K.; Dietrich, P.; Schwentner, N. *J. Chem. Phys.* **1999**, *111*, 2123. (b) Dietrich, P.; Schwentner, N. *J. Chem. Phys.* **1999**, *111*, 2133.

(13) Fuke, K.; Saito, T.; Kaya, K. *J. Chem. Phys.* **1984**, *81*, 2591.

(14) Yamanouchi, K.; Fukuyama, J.; Horiguchi, H.; Tsuchiya, S.; Fuke, K.; Saito, T.; Kaya, K. *J. Chem. Phys.* **1986**, *85*, 1806.

(15) (a) Yamanouchi, K.; Isogai, S.; Okunishi, M.; Tsuchiya, S. *J. Chem. Phys.* **1988**, *88*, 205. (b) Tsuchizawa, T.; Yamanouchi, K.; Tsuchiya, S. *J. Chem. Phys.* **1988**, *89*, 4646.

(16) Van Zee, R. D.; Blankespoor, S. C.; Zwier, T. S. *Chem. Phys. Lett.* **1989**, *158*, 306.

(17) Roncero, O.; Beswick, J. A.; Halberstadt, N.; Soep, B. In *Dynamics of Polyatomic van der Waals Complexes*; Halberstadt, N., Janda, K., Eds.; Plenum Press: New York, 1990; p 470.

(18) Zúñiga, J.; Bastida, A.; Requena, A.; Halberstadt, N.; Beswick, J. A. *J. Chem. Phys.* **1993**, *98*, 1007 and references therein.

(19) Okunishi, M.; Yamanouchi, K.; Tsuchiya, S. *J. Chem. Phys.* **1992**, *97*, 2305.

(20) Martrenchard-Barra, S.; Jouvet, C.; Lardeux-Dedonder, C.; Solgadi, D. *J. Chem. Phys.* **1993**, *98*, 5281.

(21) (a) McCaffrey, J. G.; Kerins, P. N. *J. Chem. Phys.* **1997**, *106*, 7885. (b) Kerins, P. N.; McCaffrey, J. G. *J. Chem. Phys.* **1998**, *109*, 3131.

(22) (a) Krylov, A. I.; Gerber, R. B.; Apkarian, V. A. *Chem. Phys.* **1994**, *189*, 261. (b) Krylov, A. I.; Gerber, R. B. *Chem. Phys. Lett.* **1994**, *231*, 395.

(23) Last, I.; George, T. F.; Fajardo, M. E.; Apkarian, V. A. *J. Chem. Phys.* **1987**, *87*, 5917.

(24) Tully, J. C. *J. Chem. Phys.* **1990**, *93*, 1061.

(25) Hammes-Schiffer, S.; Tully, J. C. *J. Chem. Phys.* **1994**, *101*, 4657.

(26) Aziz, R. A.; Slaman, M. J. *Mol. Phys.* **1986**, *58*, 679.

(27) Bastida, A.; Zúñiga, J.; Requena, A.; Halberstadt, N.; Beswick, J. A. *Faraday Discuss.* **1994**, *97*, 131.

(28) Batista, V. S.; Coker, D. F. *J. Chem. Phys.* **1996**, *105*, 4033.

(29) Batista, V. S.; Coker, D. F. *J. Chem. Phys.* **1997**, *106*, 6923.

(30) Bergsma, J. P.; Berens, P. H.; Wilson, K. R.; Fredkin, D. R.; Heller, E. J. *J. Phys. Chem.* **1984**, *88*, 612.

(31) Zadoyan, R.; Li, Z.; Martens, C. C.; Apkarian, V. A. *J. Chem. Phys.* **1994**, *101*, 6648 and references therein.

(32) Helbing, J.; Chergui, M.; Fernandez-Alberti, S.; Echave, J.; Halberstadt, N.; Beswick, J. A. *Phys. Chem. Chem. Phys.* **2000**, *2*, 4131.

(33) Rojas-Lorenzo, G.; Rubayo-Soneira, J.; Vigliotti, F.; Chergui, M. *Phys. Rev.* **2003**, *B67*, 15119.

(34) Berendsen, H. J. C.; Postma, J. P. M.; van Gunsteren, W. F.; DiNola, A.; Haak, J. R. *J. Chem. Phys.* **1984**, *81*, 3684.

(35) Tully, J. C. *Faraday Discuss.* **1998**, *110*, 1.

(36) Kohen, D.; Stillinger, F. H.; Tully, J. C. *J. Chem. Phys.* **1998**, *109*, 4713.